Mixed transverse modes in coupled-cavity VCSELs

Leszek Frasunkiewicz[a,b]*, Tomasz Czyszanowski[a], Kent Choquette[c], Krassimir Panajotov[b,d]

[a]Institute of Physics, Technical University of Lodz, ul. Wolczanska 219, 90-924 Lodz, Poland
[b]Vrije Universiteit Brussel, Faculty of Engineering Sciences, Brussels Photonics Team B-PHOT, Pleinlaan 2, 1050 Brussels, Belgium
[c]University of Illinois at Urbana-Champaign, Urbana, IL 61801 USA
[d]Institute of Solid State Physics, 72 Tzarigradsko Chaussee Boulevard, 1784 Sofia, Bulgaria

ABSTRACT

We present experimental results showing alternating lasing and non-lasing regions for the short-wavelength longitudinal mode in a GaAs-based 850 nm coupled-cavity vertical-cavity surface-emitting laser (CC-VCSEL). These regions are situated between the laser threshold and roll-off for this mode. The analyzed structure consists of two identical AlGaAs cavities with GaAs quantum wells, separated with 11.5 pairs of middle DBR. The current apertures are realized by ion-implantation for the top cavity and selective oxidation for the bottom cavity. We then perform fully-vectorial three-dimensional cold-cavity optical simulations to theoretically investigate optical density radial and on-optical-axis profiles of the first order transverse modes corresponding to the two longitudinal modes. We show that the short-wavelength fundamental mode λ_S-LP_{01} is subject to periodic changes of its optical field distribution when changing the oxide aperture radius, which can lead to weaker resonance of the short-wavelength LP01 mode within the coupled cavity structure.

Keywords: numerical simulation, Vertical-Cavity Surface-Emitting Laser, coupled cavities, 850 nm light emitter

1. INTRODUCTION

Vertical-cavity surface-emitting lasers (VCSEL) gathered great interest as a light-sources for cost-effective optical systems thanks to their beneficial manufacturing properties such as 2-D array mass production and on wafer-testing, as well as performance features including low power consumption, single longitudinal mode operation and circular beam emission [1]-[4]. The design considered in this paper is a coupled-cavity (CC-) VCSEL, which possesses two optical cavities separated by a middle disturbed Bragg reflector (DBR) and has been first realized by Stanley *et al.* in [5]. Such structures support two longitudinal modes with a spectral difference defined by the cavity detuning and the middle DBR transmissivity [5], [6]. Ability to apply different currents to the cavities allows for the two longitudinal modes, usually named after their wavelength - short and long, to be emitted independently or simultaneously [7]-[12]. The CC-VCSEL structures allows utilizing one of the cavities as an active lasing source and the other one as a modulator based on electro-absorption, or electro-refraction phenomena. Such additional flexibility can be used to achieve wavelength switching or voltage-controlled polarization switching [13]-[15]. VCSELs are generally complex structures and are a challenging subject for theoretical and numerical analysis. Adding other degrees of freedom in the form of a second cavity and an additional DBR, makes understanding of the physical phenomena occurring in CC-VCSELs considerably more complicated. In this paper we present an unexpected and difficult to explain experimental result on alternating lasing and non-lasing regions for the short-wavelength longitudinal mode of GaAs CC-VCSELs. We then utilize an advanced fully-vectorial three-dimensional optical model to find the reason for the observed phenomenon.

2. CC-VCSEL STRUCTURE

Our study is based on CC-VCSEL structure emitting at 850 and 861 nm wavelengths (Fig. 1). The multi-quantum well

Semiconductor Lasers and Laser Dynamics VII, edited by Krassimir Panajotov, Marc Sciamanna, Angel Valle, Rainer Michalzik, Proc. of SPIE Vol. 9892, 989221 · © 2016 SPIE
CCC code: 0277-786X/16/$18 · doi: 10.1117/12.2227845

active regions within the two identical 1-λ AlGaAs cavities consist of five 10-nm-thick GaAs quantum wells separated by 9-nm-wide $Al_{0.2}Ga_{0.8}As$ barriers. The DBRs are made of $Al_{0.16}Ga_{0.84}As/Al_{0.92}Ga_{0.08}As$. The top one consists of 21 DBR pairs, the middle one of 13.5 pairs and the bottom one of 35 pairs. The electrical aperture for the bottom cavity of 2 μm radius is realized by selectively oxidized layer on the top side of the bottom cavity. For the top cavity, the current confinement of 4 μm radius is defined by ion implantation of the top DBR. The oxide aperture is also responsible for the transverse optical confinement in the structure and due to its small dimensions, the laser is nominally a single transverse mode device.

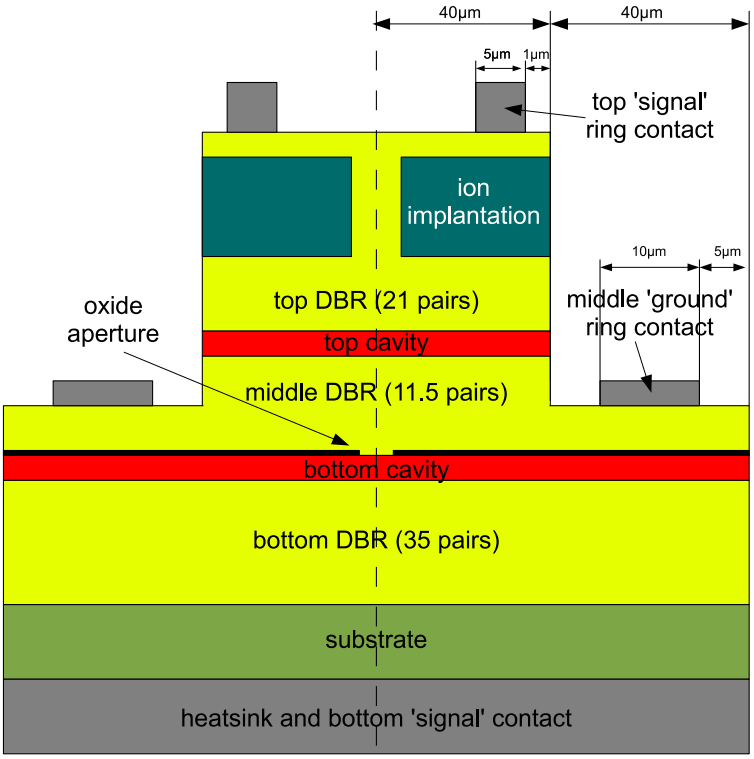

Figure 1. Schematic view (cross sections in the *rz* plane) of the analyzed CC-VCSEL structure.

3. EXPERIMENT

In the experiment we are biasing the top cavity with a constant current I_{TOP} and checking which longitudinal modes lase when changing the bottom injection current I_{BOT} within 0-10 mA range. For I_{TOP} = 6 mA we have observed alternating lasing and non-lasing regions between the short-wavelength mode threshold and roll-off currents (Fig. 2). For certain values of the current injected into the bottom cavity I_{BOT}, the short-wavelength longitudinal mode suddenly disappears. These regions of short-wavelength mode absence are happening for a narrow range of currents, yet are very well defined and repeatable.

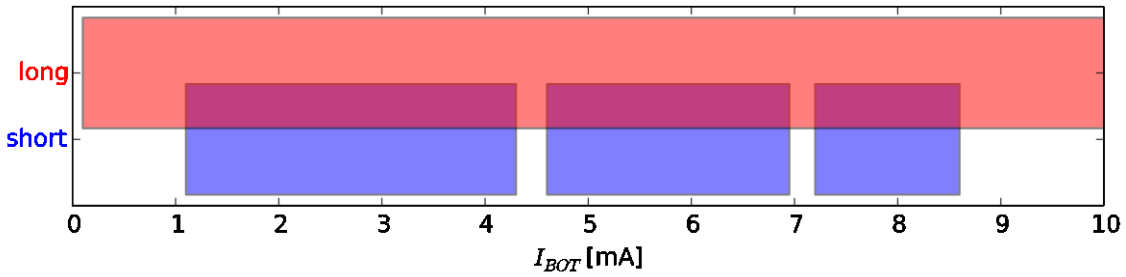

Figure 2. (color online) Bottom current values at a constant top bias current I_{TOP} = 6 mA, for which short-wavelength (blue regions) and long-wavelength (red region) longitudinal modes lase. The regions are thick and overlap to show that both modes lase simultaneously.

4. SIMULATIONS

4.1 Model

Due to the nature of experimentally observed short-wavelength mode non-lasing regions, we have initially excluded phenomena that change monotonically with current increase from the pool of possible reasons for obtained behavior. We have come up to a conclusion that the most probable source of such perturbations lies in the transverse optical confinement that changes due to thermal lensing effect. With such an assumption we could simplify our analysis to purely optical, cold cavity simulations, substituting the thermal focusing by widening of the oxide aperture. Our numerical procedure is based on a fully-vectorial 3-dimensional plane wave admittance method as described in [16-18], which is capable of finding resonant modes in complicated vertically-stacked laser structures. Plane-wave decomposition for this analysis is done using 882 plane-waves in each layer of the structure.

In the simulations we used the set of parameters as listed in Table 1.

Table 1. Refractive indices at 300 K and for wavelength of 854 nm used in the simulations.

	REFRACTIVE INDEX	
Material	Value	Ref.
GaAs	3.591	[19-20]
$Al_{(0.11)}Ga_{(0.89)}As$	3.521	[19-21]
$Al_{(0.16)}Ga_{(0.84)}As$	3.489	
$Al_{(0.20)}Ga_{(0.80)}As$	3.464	
$Al_{(0.37)}Ga_{(0.63)}As$	3.357	
$Al_{(0.57)}Ga_{(0.43)}As$	3.231	
$Al_{(0.60)}Ga_{(0.40)}As$	3.213	
$Al_{(0.76)}Ga_{(0.24)}As$	3.113	
$Al_{(0.79)}Ga_{(0.21)}As$	3.094	
$Al_{(0.92)}Ga_{(0.08)}As$	3.013	
$Al_{(0.98)}Ga_{(0.02)}As$	2.976	
AlOx	1.537	[22]

4.2 Results

We have analyzed the wavelength and modal loss dependencies on the oxide aperture radius for the LP_{01} short-wavelength and long-wavelength modes. It can be seen in Fig. 3 that the fundamental long-wavelength mode λ_L-LP_{01} shows tendency similar to the one observed in regular VCSELs. On the other hand, the short-wavelength fundamental mode λ_S-LP_{01} experiences periodic perturbations including regions of greatly increased modal losses.

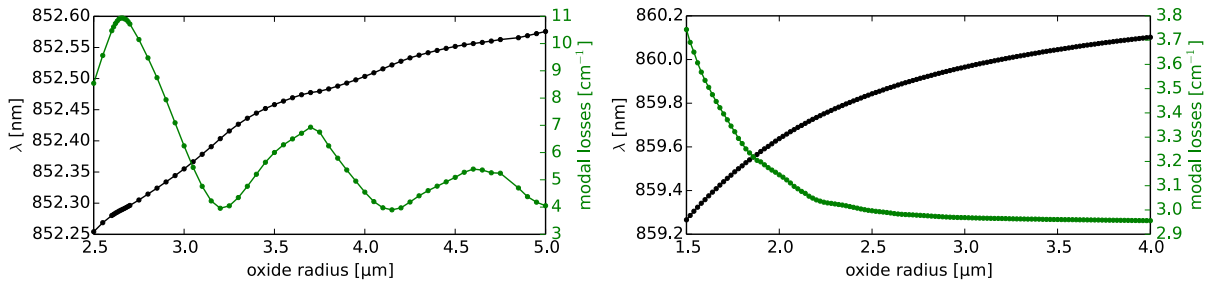

Figure 3. (color online) Wavelength (black) and modal losses (green) dependencies on the oxide-aperture radius for the short-wavelength (left) and long-wavelength (right) fundamental mode.

Next, we have checked the radial and the longitudinal (on-optical-axis or z-) optical intensity profiles of both modes for oxide aperture radii correlated with the short-wavelength fundamental mode losses extrema (Fig. 4). It can be seen that the long-wavelength mode maintains its typical Gaussian shape in both cavities with size adjusted to the oxide radius. Additionally, its *z*-profile stays practically unchanged, showing a well-defined standing wave. The situation differs significantly for the short-wavelength mode (shown with blue lines in Fig.4), which changes its radial and longitudinal profiles when the oxide-aperture radius is varied. These changes have a periodic character and include two well-distinguishable states:

1. A Gaussian-like transverse-profile and a longitudinal-profile with two maxima situated in the two cavities (Figs 4a,c and 5b). We call this a PP (Peak-Peak) configuration. In this state, the *z*-profile shows non-zeroing intensity values at the boundaries between the middle DBR layers, indicating weaker mode resonance. Such occurrences correlate with the modal losses maxima.
2. Transverse-profile with a maximum in one cavity and a non-zero minimum in the middle of the second cavity (Figs 4b and 5a,c). We call this a PH/HP (Peak-Hole/Hole-Peak) configuration. In such a state the standing-wave pattern is well formed and it correlates with modal loss minima.

A full period of modal changes consists of PP-HP-PP-PH-PP states with smooth modal profile changes between them.

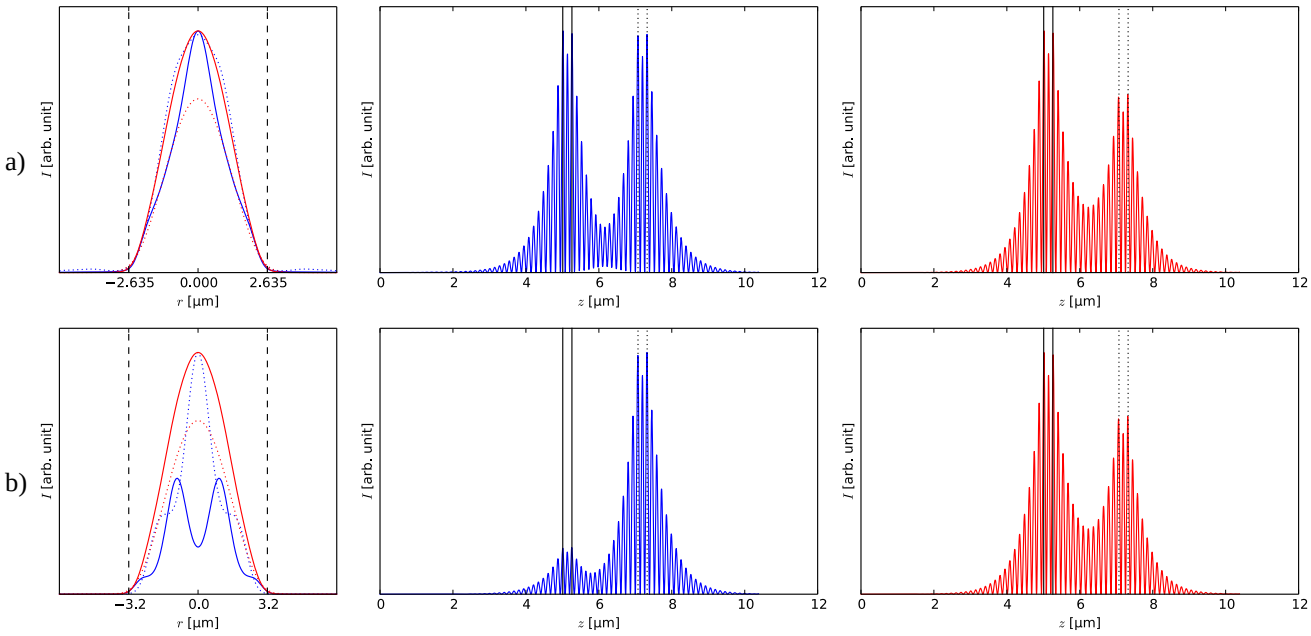

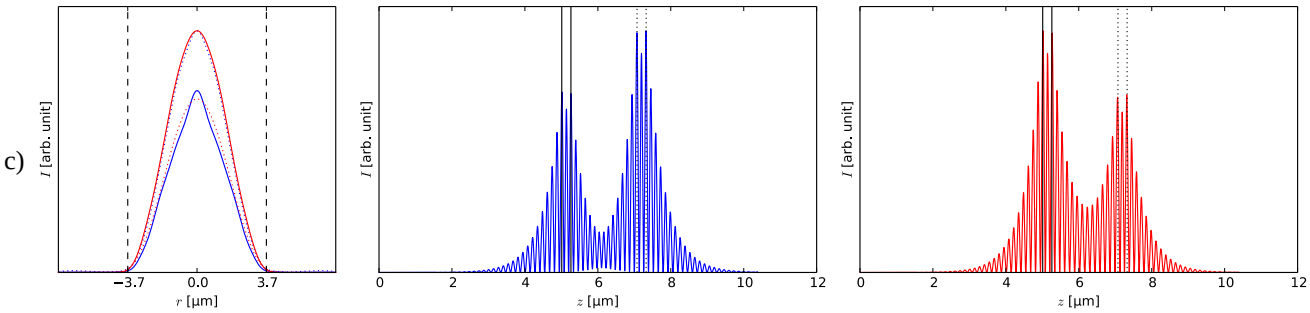

Figure 4. (color online) Each row represents a set of short-wavelength (blue) and long-wavelength (red) mode radial (left) and longitudinal (middle and right) profiles for different oxide aperture radii: a) 2.635, b) 3.2 and c) 3.7 μm are shown. Left graphs depict radial mode profiles with continuous (dotted) line showing the profile in the bottom (top) cavity and vertical dashed lines indicating the oxide aperture radius. Middle and right graphs show longitudinal intensity profiles with vertical continuous (dotted) lines indicating bottom (top) cavity boundaries.

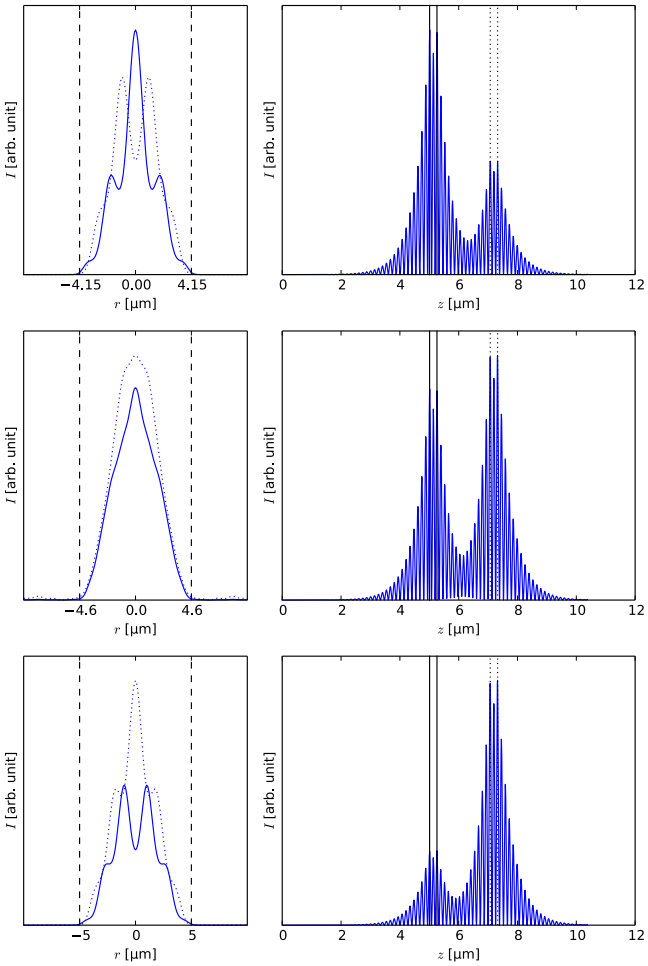

Figure 5. Each row shows the short-wavelength mode radial (left) and longitudinal (right) profiles for different oxide aperture radii: a) 4.15, b) 4.6 and c) 5.0 μm. Left graphs depict radial mode profiles, continuous (dotted) line shows the profile in the bottom (top) cavity, vertical dashed lines indicate the oxide aperture radius. Right graphs show the longitudinal profiles, vertical continuous (dotted) lines indicate bottom (top) cavity boundaries.

5. CONCLUSIONS

Using fully-vectorial, three-dimensional, cold-cavity simulations, we have successfully explained the appearance of periodic alternating lasing and non-lasing regions of the short-wavelength mode of CC-VCSELs. We have related these regions to the changes of the transverse optical confinement radius within the CC-VCSEL. Since the oxide aperture size increase can substitute effects of increased thermal lensing, we believe, that the numerically obtained results explain the experimentally observed behavior.

ACKNOWLEDGEMENTS

This work was supported in part by FWO Vlaanderen Project G.0657.09N and OZR-VUB and in part by the Polish National Science Centre, Project DEC-2012/06/M/ST7/00442. K. P. is grateful to the Methusalem foundation for financial support.

REFERENCES

[1] Yu, S. F., [Analysis and Design of Vertical Cavity Surface Emitting Lasers], Hoboken, NJ, Wiley-VCH (2003).
[2] Numai, T., [Fundamentals of semiconductor lasers], Springer, Kusatsu, Japan (2004).
[3] Sale, T. E., [Vertical cavity surface emitting lasers], Research Studies Press Taunton, Great Britain (1995).
[4] Coldren, L. A., Corzine, S. W. and Mashanovitch, M. L., [Diode lasers andphotonic integrated circuits], Hoboken, NJ, Wiley (2012).
[5] Stanley, R., Houdre, R., Oesterle, U., Ilegems, M., and Weisbuch, C., "Coupled semiconductor microcavities," Appl. Phys. Lett., vol. 65, no. 16, 2093–2095 (1994).
[6] Pellandini, P., Stanley, R., Houdre, R., Oesterle, U., Ilegems, M. and Weisbuch, C., "Dual-wavelength laser emission from a coupled semiconductor microcavity," Appl. Phys. Lett., vol. 71, no. 7, 864–866 (1997).
[7] Michler, P., Hilpert, M. and Reiner, G., "Dynamics of dual-wavelength emission from a coupled semiconductor microcavity laser," Appl. Phys. Lett., vol. 70, no. 16, 2073–2075 (1997).
[8] Carlin, J., Stanley, R., Pellandini, P., Oesterle, U., and Ilegems, M., "The dual wavelength bi-vertical cavity surface-emitting laser," Appl. Phys. Lett., vol. 75, no. 7, 908–910 (1999).
[9] Fischer, A., Choquette, K., Chow, W., Hou, H. and Geib, K., "Coupled resonator vertical-cavity laser diode," Appl. Phys. Lett., vol. 75, no. 19, 3020–3022 (1999).
[10] Brunner, M., Gulden, K., Hovel, R., Moser, M., Carlin, J., Stanley, R. and Ilegems, M., "Continuous-wave dual-wavelength lasing in a two-section vertical-cavity laser," IEEE Photonics Technol. Lett., vol. 12, no. 10, 1316–1318, (2000).
[11] Badilita, V., Carlin, J.-F., Ilegems, M. and Panajotov, K., "Rate-equation model for coupled-cavity surface-emitting lasers," IEEE J. Quantum Electron., vol. 40, no. 12, 1646–1656 (2004).
[12] Badilita, V., Carlin, J.-F., Brunner, M. and Ilegems, M., "Light-current characterization of dual-wavelength vcsels," Symposium on Integrated Optoelectronic Devices., 87–95 (2002).
[13] Badilita, V., Carlin, J.-F., Ilegems, Brunner, M., Verschaffelt, G. and Panajotov, K., "Control of polarization switching in vertical coupled cavities surface emitting lasers," IEEE Photonics Technol. Lett., vol. 16, no. 2, 365–367 (2004).
[14] Grasso, D. M. and Choquette, K. D., "Temperature-dependent polarization characteristics of composite-resonator vertical-cavity lasers," IEEE J. Quantum Electron., vol. 41, no. 2, 127–131 (2005).
[15] Panajotov, K., Zujewski, M. and Thienpont, H., "Coupled-cavity surface-emitting lasers: spectral and polarization threshold characteristics and electrooptic switching," Optics Express, vol. 18, no. 26, 27 525–27 533 (2010).
[16] Dems, M., Chung, I.-S., Nyakas, P., Bischoff, S. and Panajotov, K., "Numerical methods for modeling Photonic-Crystal VCSELs," Opt. Express, vol. 18, 16042 (2010).
[17] Panajotov, K., Dems, M. and Czyszanowski, T., [Compact Semiconductor Lasers], Wiley-VCH Verlag GmbH & Co. KGaA, Weinheim, chapt. 4 (2014).
[18] Dems, M., Kotynski, R. and Panajotov, K., "Plane Wave Admittance Method, a novel approach for

determining the electromagnetic modes in photonic structures," Opt. Express, vol. 13, 3196 (2005).
[19] Marple, D. T. F., "Refractive Index of GaAs," J. Appl. Phys., vol. 35, no. 4, 1241-1242 (1964).
[20] Adachi, S., [Properties of Semiconductor Alloys: Group-IV, III-V and II-VI Semiconductors], Wiley (2009).
[21] Gehrsitz, S., "The refractive index of $Al_xGa_{1-x}As$ below the band gap: Accurate determination and empirical modeling," J. Appl. Phys., vol. 87, no. 11, 7825 - 7837 (2000)
[22] Kitatani, T. and Kondow, M., "Characterization of the Refractive Index of Lateral-Oxidation-Formed Al_xO_y by Spectroscopic Ellipsometry," Jpn. J. Appl. Phys., vol. 41, no. 5A, 2954-2957 (2002).